T. Sawada et alii, Frattura ed Integrità Strutturale, 38 (2016) 92-98; DOI: 10.3221/IGF-ESIS.38.12

Focussed on Multiaxial Fatigue and Fracture

Effect of molding processes on multiaxial fatigue strength in short fibre reinforced polymer

Takahiko Sawada, Hiroshi Aoyama
Research & Development Group, Hitachi, Ltd.,
takahiko.sawada.dy@hitachi.com,hiroshi.aoyama.ra@hitachi.com

ABSTRACT. This study concerns the multiaxial static and fatigue strength properties. Short-glass-fibre-reinforced phenolic-resin composites (SGP) molded by injection and compression processes were subjected to tension-torsion combined static and fatigue tests at room temperature under various test conditions. Tension – torsion combined static strength well agreed with Tsai-Hill failure criteria without depending on processes. Relationships between the maximum principal stress, $\sigma_{p1,\,max}$, and the number of fracture cycles, N_f, were approximately linear in the whole range of up to 10^6 cycles. For a unified evaluation of multiaxial fatigue life for SGP, non-dimensional effective stress, σ^*, defined by modifying Tsai-Hill failure criteria was applied. The slopes of σ^*- N_f curves according to Baskin's law were almost identical to the injection (n = 26.3) and compression (n = 26.2). We finally confirmed that the multiaxial fatigue life of SFRP could be predicted by using σ^* with a unique Wöhler curve without relying on molding processes.

KEYWORDS. Short-fibre reinforced plastics; Multiaxial; Fatigue; Tsai-Hill.

Citation: Sawada, T., Aoyama, H., Effect of molding processes on multiaxial fatigue strength in short fibre reinforced polymer, Frattura ed Integrità Strutturale, 38 (2016) 92-98.

Received: 27.06.2016
Accepted: 26.07.2016
Published: 01.10.2016

INTRODUCTION

Short fibre reinforced thermo-set plastic (SFRP) has been mainly applied to automobiles and electrical industries owing to its superior mechanical properties and lower weight. However, a machine designer often faces difficulties using SFRP or predicting its mechanical properties. SFRP generally shows complex fracture behaviours combined with a matrix crack, fibre break, fibre pull-out, and others, and these make product design difficult. Therefore, a machine designed using SFRP often requires a production test and a strength test to be repeated until its reliability is confirmed. Because reducing the number of test repetitions decreases the cost of development, high-reliability strength evaluation methods will be required to meet the increase in products that will use SFRP in the future.
Further, multiaxial stress generally occurs in a structure subjected to an external force. In the literature, Moosbrugger et al. [1, 2] experimentally investigated and calculated the multiaxial fatigue behaviour of SFRP. They conducted some tension-torsion combined fatigue tests and estimated the fatigue life on the basis of the failure criterion of laminate. Gaier et al. [3] established a simulation process for the multiaxial fatigue life prediction of orthotropic SFRP. They combined the resin flow simulation, finite element analysis, and fatigue analysis. The fatigue damage of a belt pulley was predicted by

comparing experimental and simulation results. Although some additional papers [4-7] have focused on investigating the multiaxial strength for SFRP, little attention has been paid to the effect of manufacturing process on that property.
This study is concerned with the multiaxial fatigue evaluation in short-glass-fibre reinforced phenolic resin (SGP) among various volume fractions. Round-bar specimens molded by injection and compression processes were subjected to static and fatigue tests in room temperqature to clarify the effect of molding processes on the multiaxial strength. Tension - torsion combined tests were conducted with various stress ratio parameters described as the ratio of torsion and tension stress as $a = \tau / \sigma$.

EXPERIMENTAL DETAILS

Tab. 1 details the configuration of SGP. Thermosetting phenolic resin was used as the matrix. The reinforcement was a short E-glass fibre 10 mm long and 10 μm in diameter. $0.0V_f$, $0.2V_f$, and $0.5V_f$ described at the first row means that the fiber volume fraction V_f is 0%, 20%, and 50%.
Test specimens with three-types V_f were molded by compression (C-SGP) and injection (I-SGP) respectively. In the compression molding, 300-mm-square and 30-mm-thick bulk plates were manufactured, and then test pieces were cut from the bulk plate to the dimensions as shown in Fig. 1. Edges of the sample surface were not polished. A machining surface roughness was confirmed by using a roughness tester to be approximately the same in each specimen. Compression molding temperature was 160 °C, press pressure was 20 MPa, and curing time was 250 seconds. In contrast, in injection molding, test specimens were directly manufactured to specimen shapes described as Fig.1. Injection mold temperature was 140-160 °C, injection pressure was 80 MPa, and curing time was 20 seconds.

Component		$0.0V_f$	$0.2V_f$	$0.5V_f$
Glass Fibre	[%]	0	20	50
Phenolic resin	[%]	70~85	55~65	30~35
Phenol	[%]	1	1	1
Hexamethylene etramine	[%]	3	3	3
Rock wool	[%]	10~20	10~20	10~20
Zinc stearate	[%]	1.0~2.0	1.0~2.0	10~20

Table 1: Configuration of SGP material.

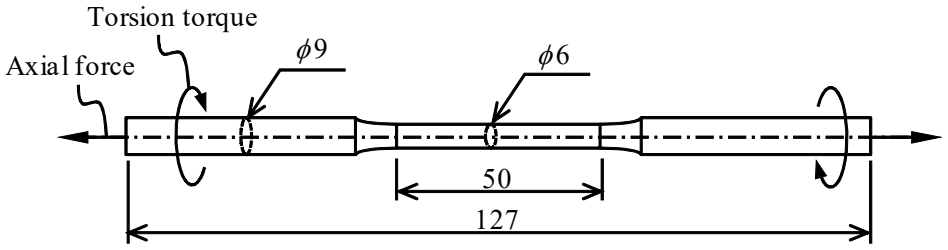

Figure 1: Tension-torsion test specimen dimensions.

Multiaxial test procedure
In this study, we conducted multiaxial static and fatigue tests at room temperature to compare strength properties in different manufacturing processes. All the tests were performed by combining tension-torsion electro-hydraulic servo systems under axial-loads up to ± 25 kN with standard displacements of ± 50 mm and torsion-torques up to 220 N·m with total rotations of 270°.
Tension-torsion combined tests were performed by using the specimen as shown in Fig. 1. Tension stress σ_1 is given by Eq. 1, where F is tension load and D is diameter at the gauge section. Torsion stress τ_{12} is given by Eq. 2, where T is torque.

$$\sigma_1 = \frac{4F}{\pi D^2} \tag{1}$$

$$\tau_{12} = \frac{16T}{\pi D^3} \tag{2}$$

Axial-tension stress σ_1 was loaded in proportion to torsion stress τ_{12} in accordance with a combined stress ratio a, which is defined in Tab. 2, on the gauge section surface. Static tests were controlled by Eq. 3 so as to achieve the stress loading speed ($\dot{\sigma}$, $\dot{\tau}$) of 10 MPa/sec. Fatigue tests were conducted at the stress ratio R defined as the ratio of minimum stress to maximum stress of 0.1 and applied sinusoidal waves combined between axial-tension stress and torsion stress with cyclic frequency f of 2 Hz. Axial-tension stress was loaded to the specimen so as to be in the same phase with torsion stress in accordance with defined the combined stress ratio a in Tab. 2.

τ_{12}	σ_1	$a=\tau_{12}/\sigma_1$
1	0	1/0 (pure torsion)
1	1	1/1
1	2	1/2
0	1	0/1 (pure tension)

Table 2: Definitions of combined stress ratio a.

$$\sqrt{\dot{\sigma}^2 + \dot{\tau}^2} = 10 \ [\text{MPa} / \text{sec}] \tag{3}$$

TEST RESULTS AND DISCUSSION

Multiaxial static strength evaluation

External load acting on a structure is commonly considered to be not only a uni-axial stress but also a multiaxial stress state. Therefore, we discuss a multiaxial strength criterion in terms of the axial tension strength and the torsional shear strength in this chapter.

From the micro observation and frequency analysis for fibre orientation in C-SGP and I-SGP, we deduced that they will have an orthotropic property. Then, we assumed the SGP multiaxial failure was followed by Tsai-Hill failure criterion given by Eq. 4 [8].

$$\frac{\sigma_1^2}{\sigma_L^2} + \frac{\tau_{12}^2}{\tau_S^2} = 1 \tag{4}$$

where σ_L and τ_S are tension and torsional strength in material reference axes, and σ_1, and τ_{12} are applied axial stress and torsional stress on the specimen surfaces. Suffixes 1 and 12, which are written in subscript to the right of strength parameters σ and τ, indicate the axial-stress direction and the torsional-stress direction, respectively. σ_L and τ_S are the material strengths determined by the static test on the basis of the experimental results in a = 0 / 1 and a = 1 / 0 in Tab. 2. Fig. 2 shows the static strength criterion for SGP in the multiaxial stress state, which is plotted on σ_L - τ_S plane. The white and gray plots on each chart indicate the strength data of C-SGP and I-SGP, respectively. The solid lines on the σ - τ plane represent the failure criterion given by Eq. 4 for each V_f. Broken lines represent a given in Tab. 2.

As C-SGP is molded by pressuring and heating after raw materials described at Tab. 1 are filled into the die, a microscopic void tends to be easily retained as a manufacturing defect in C-SGP. Furthermore, the authors [9] previously suggested that the strength properties of SGP depend on both short-fibres orientation and manufacturing defects in matrices. From these perspectives, we deduced that these manufacturing defects affected experiment variations in SGP. Considering such manufacturing defects, the static fracture strength of C-SGP approximately accords with the Tsai-Hill failure theory criteria in Eq. 4.

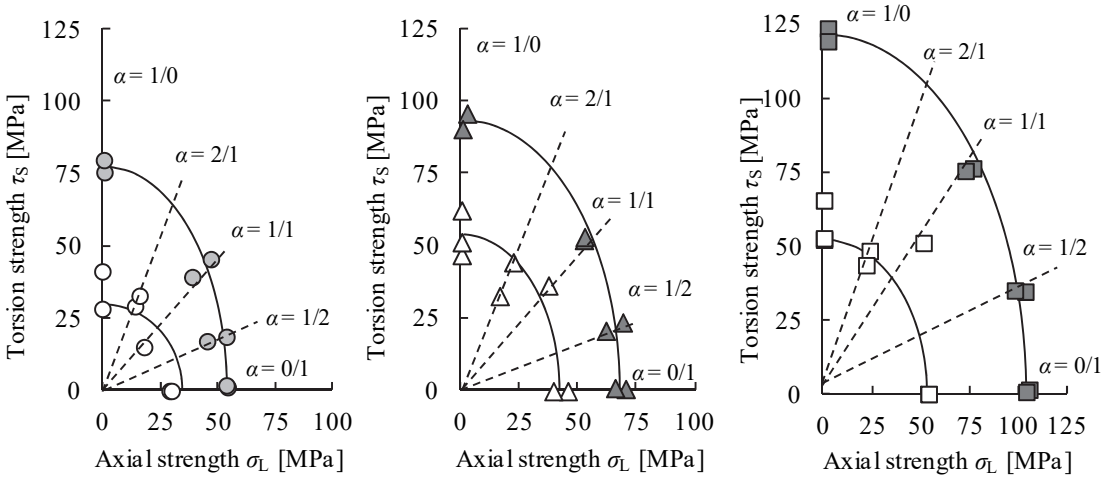

Figure 2: Multiaxial static strength evaluation with Tsai-Hill failure rule.

Fatigue strength properties

Fatigue strength in uni-axial loading is generally evaluated by using the S-N diagram. S-N diagrams are associated with the relationships among the number of cycles to failure and stress range, stress amplitude, or maximum stress in uni-axial loading. However, we have to deal with stress states of combined axial stress and torsion stress in this paper. Therefore, S-N diagrams are organized by using principal stress applied on specimen surfaces σ_{p1}, and the number of cycles to fracture N_f. σ_{p1} was calculated as follows:

$$\sigma_{p1} = \frac{\sigma_1}{2} + \sqrt{\left(\frac{\sigma_1}{2}\right)^2 + \tau_{12}^2} \tag{5}$$

where σ_1 and τ_{12} are the axial stress and shear stress applied.

Figs 3 and 4 show the relationships between $\sigma_{p1,max}$ as cyclic maximum principal stress and N_f as fracture cyclic numbers on a double logarithmic chart obtained as S-N diagrams. Arrows in the diagrams show that the fatigue tests were terminated after reaching 1×10^6 cycles.

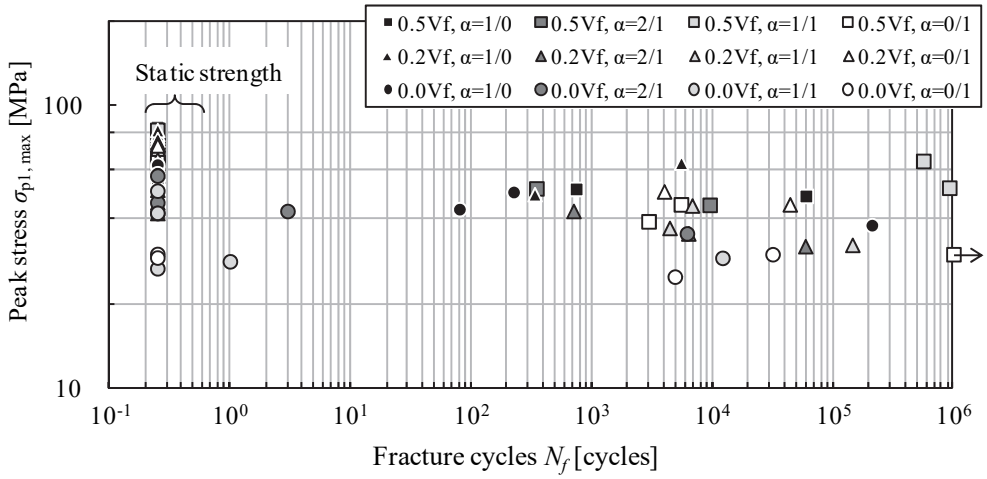

Figure 3: Relationships between $\sigma_{p1,max}$ and N_f with various a in C-SGP.

Since the value of the fatigue life in C-SGP are scattered widely, fatigue life in C-SGP can no longer be expected to sort in V_f and a by using the S-N diagram. Meanwhile, S-N diagram in I-SGP indicates the characteristic to decrease $\sigma_{p1,max}$ with increasing N_f without dependence on fatigue test conditions. Comparing the fatigue properties in molding processes, they

do not seem to agree despite these properties being made of the same materials. V_f, a, and molding processes strongly affect the multiaxial fatigue properties, hence those effects have to be removed from S-N diagrams to evaluate fatigue with high accuracy.

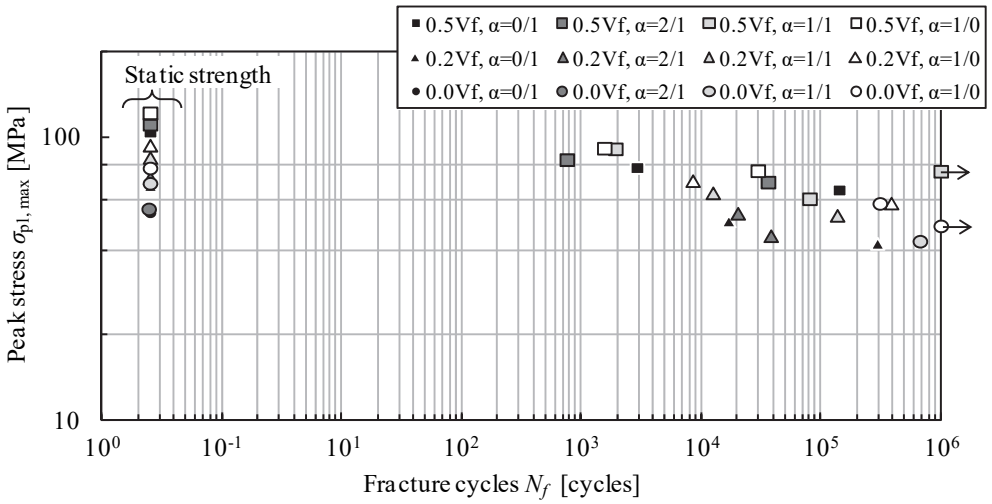

Figure 4: Relationships between $\sigma_{p1,\,max}$ and N_f with various a in I-SGP.

Definition of unified equivalent stress

We confirmed multiaxial fracture strengths well agreed with the Tsai-Hill failure criteria with dependence on processes and fibre volume fractions V_f as shown in Fig. 2. Meanwhile, multiaxial fatigue properties are not able to be organized by the relationships between $\sigma_{p1,max}$ and N_f because of being affected the dependence on the molding process, a, and V_f.
Then, due to the static strength behaviours described above, the fatigue strength will be represented by expanding the Tsai-Hill failure rule [10]. Hence, non-dimensional equivalent stress σ^* was defined by modifying the Tsai-Hill failure rule as shown in Eq. 6 to evaluate the multiaxial fatigue behaviour without dependence on molding process effects.

$$\sqrt{\frac{\sigma_1^2}{\sigma_L^2}+\frac{\tau_{12}^2}{\tau_S^2}}=\sigma^* \tag{6}$$

Figs 5 and 6 show the relationships between σ^* and N_f on double logarithmic charts in C-SGP and I-SGP. σ^*- N_f correlation is approximately determined by Baskin's law [11] with the broken line in Fig. 6. Baskin's law is presented by Eq. 7 as follows;

$$N_f\left(\sigma^*\right)^n=C \tag{7}$$

where n and C are presented as material constants for a slope of σ^*- N_f correlation on the double logarithmic chart.
The slopes of σ^* - N_f curves represented by Baskin's law were almost identical for the C-SGP (n = 26.2) and I-SGP (n = 26.3). Comparing σ^*-N_f curves among the manufacturing processes, fatigue strengths in C-SGP are widely fluctuated than that of I-SGP. Fig. 7 shows typical fracture surface observation image in C-SGP by scanning electron microscopy. Manufacturing defects like a cavity were able to be observed on the fracture surface area, and it is deduced that they became the origin of the fatigue failure. Therefore it is considered that the manufacturing processes were affected on the strength distribution. Although C-SGP shows wider fatigue life distributions than I-SGP, we are practically able to predict fatigue life by using σ^* considering the strength variation that depends on the manufacturing defects. The proposed method is expected to be applied to the fatigue life estimation as a unified evaluation method in SGP without depending on manufacturing processes. Therefore, σ^* - N_f correlation is synthetically able to evaluate the multiaxial fatigue properties without dependence on molding processes, fibre volume fraction, and combined stress ratio a.

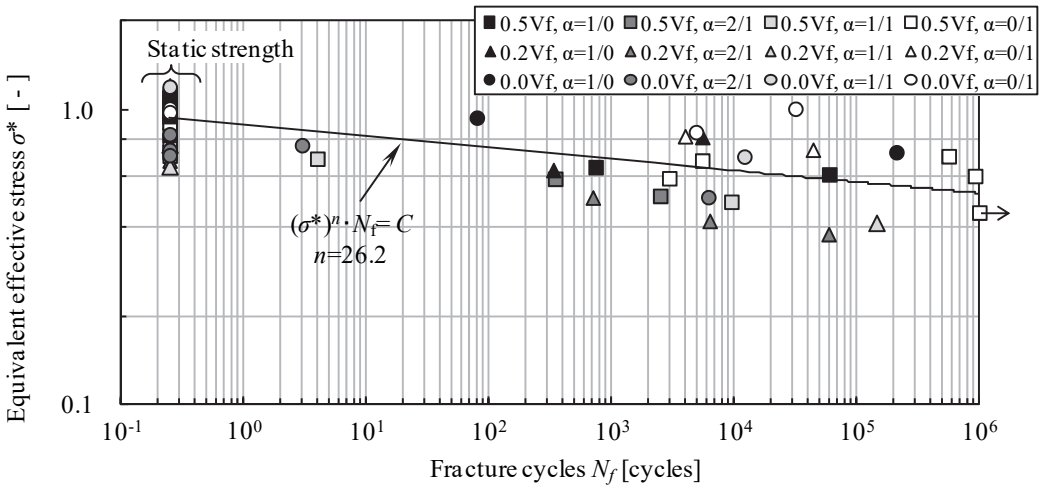

Figure 5: Relationships between σ^* and N_f with various a in C-SGP.

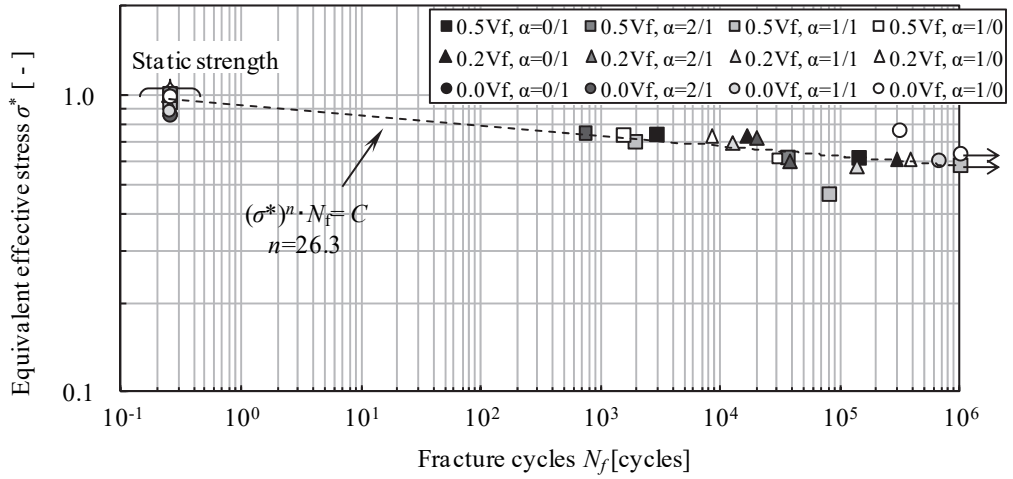

Figure 6: Relationships between σ^* and N_f with various a in I-SGP.

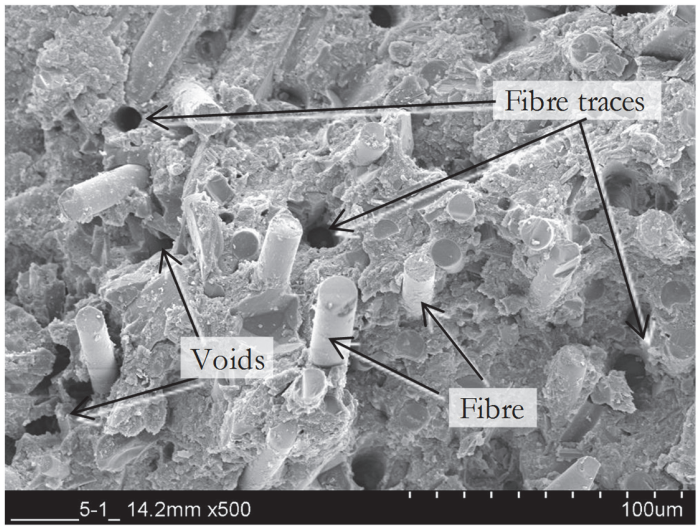

Figure 7: A typical tensile fracture surface situations with scanning electron microscopes in C-SGP. (05V_f)

CONCLUSIONS

Multiaxial fatigue evaluation in SGP among the various volume fractions was investigated in this paper. Round-bar specimens molded by injection and compression processes were subjected to static and fatigue tests in room temperature to clarify the effect of molding processes on the multiaxial strength. Tension - torsion combined tests were conducted with various combined stress ratio parameters described as $a = \tau / \sigma$. General conclusions of this study are as follows.

1. Tsai-Hill failure criteria can be applied to evaluate tension-torsion static strength in SGP with dependence on the molding process and V_f.
2. The non-dimensional equivalent stress σ^* is defined to evaluate multiaxial fatigue strength by modifying Tsai-Hill failure criteria.
3. The slopes of σ^*- N_f curve for I-SGP (n = 26.3) is almost identical to that for C-SGP (n = 26.2).
4. The relationship between σ^* and N_f explains the tension-torsion fatigue properties on the double logarithmic chart without depending on a molding process, combined stress ratios a, and fibre volume fraction V_f especially for I-SGP.

REFERENCES

[1] Sonsino, C.M., Moosbrugger, E., Fatigue design of highly loaded short-glass-fibre reinforced polyamide parts in engine compartments, Int. J. Fatigue, 30 (2008) 1279-1288.
[2] Moosbrugger, H., Demonte, M., Multiaxial fatigue behavior of a short-fiber reinforced polyamide–experiments and calculations, Mat.-wiss. U. Werkstofftech, 42 (2011) 950-957.
[3] Gaier, C., Unger, B., Dannbauer, H., Multiaxial fatigue analysis of orthotropic materials, Revue de Metallurgie, 107 (2010) 369-375.
[4] Quaresimin, M., Susmel, L., Talreja, R., Fatigue behaviour and life assessment of composite laminates under multiaxial loading, Int. J. Fatigue, 32 (2010) 2-16.
[5] Launay A., Maitournam M.H., Marco Y., Raoult I., Multiaxial fatigue models for short glass fiber reinforced polyamide – Part I: Nonlinear anisotropic constitutive behavior for cyclic response, Int. J. Fatigue, 47 (2013) 382-389.
[6] Launay, A., Maitournam, M.H., Marco, Y., Raoult, I., Multiaxial fatigue models for short glass fibre reinforced polyamide. Part II: Fatigue life estimation, Int. J. Fatigue, 47 (2013) 390-406.
[7] Klimkeit, B., Nadot, Y., Castagnet, S., Nadot-Martin, C., Dumas, C., Bergamo, S., Multiaxial fatigue life assessment for reinforced polymersOriginal, Int. J. Fatigue, 33 (2011) 766-780.
[8] Tsai, S.W., Strength Characteristics of Composite Materials, NASA CR-224, (1965).
[9] Sawada, T., Aoyama, H., Effect of molding process on mechanical properties of glass short fiber/phenolic resin composite, Trans. Soc. Mech. Eng. A Japan, 76 (2009) 672-674.
[10] Kawai, M., Yajima, S., Takano, Y., Off-axis Fatigue and Its Damage Mechanics Modeling for Unidirectional Carbon Fiber-Reinforced Composite at Room and High Temperatures, Trans. Soc. Mech. Eng. A Japan, 64 (1998) 2838-2864.
[11] Basquin, O. H., The experimental law of endurance tests, Proceedings of ASTM, 10 (1910) 625-630.